PHYSICAL REVIEW C **84**, 061303(R) (2011)

Coulomb excitation of ^{124,126,128}Sn

J. M. Allmond,[1] D. C. Radford,[2] C. Baktash,[2,*] J. C. Batchelder,[3] A. Galindo-Uribarri,[2,4] C. J. Gross,[2] P. A. Hausladen,[1] K. Lagergren,[1] Y. Larochelle,[4] E. Padilla-Rodal,[1,†] and C.-H. Yu[2]

[1]*Joint Institute for Heavy Ion Research, Oak Ridge National Laboratory, Oak Ridge, Tennessee 37831, USA*
[2]*Physics Division, Oak Ridge National Laboratory, Oak Ridge, Tennessee 37831, USA*
[3]*UNIRIB, Oak Ridge Associated Universities, Oak Ridge, Tennessee 37831, USA*
[4]*Department of Physics and Astronomy, University of Tennessee, Knoxville, Tennessee 37996, USA*

(Received 14 August 2011; published 20 December 2011)

High-precision measurements of $\langle 0_1||M(E2)||2_1\rangle$ matrix elements from the Coulomb excitation of ^{124,126,128}Sn on a ^{12}C target are presented. The extracted $B(E2)$ values decrease monotonically from the neutron midshell toward the ^{132}Sn double-shell closure, despite a near constancy in the first 2^+ level energy. Furthermore, Coulomb excitation of ^{124,126,128}Sn on an enriched ^{50}Ti target, combined with the results from the ^{12}C target, provide a measure of the static quadrupole moments, $Q(2_1{}^+)$ (expected to be zero for a spherical shape). These new results confirm that the unstable neutron-rich ^{126,128}Sn isotopes have deformations consistent with zero. The present study marks the first report on measured $2_1{}^+$ static quadrupole moments for unstable closed-shell nuclei.

DOI: 10.1103/PhysRevC.84.061303 PACS number(s): 25.70.De, 23.20.−g, 21.10.Ky, 27.60.+j

The study of nuclei far from stability, particularly with respect to shell closures [1], has become a topic of high interest with the advent of radioactive ion beams (RIBs). For example, Coulomb-excitation studies of Sn nuclei approaching the $N = 82$ neutron shell closure require the use of unstable Sn beams—cf. Fig. 1. The Sn isotopes are of special interest in that they constitute the longest double-magic ($N = Z = 50$, ^{100}Sn) to double-magic ($Z = 50, N = 82$, ^{132}Sn) isotopic chain available for nuclear structure study. They provide a unique opportunity for testing and improving shell-model theories. Closed-shell nuclei are widely assumed to be spherical in their low-lying states; testing this assumption, particularly for radioactive neutron-rich nuclei close to the ^{132}Sn double-shell closure, requires high-precision measurements of $\langle 0_1||M(E2)||2_1\rangle$ and $\langle 2_1||M(E2)||2_1\rangle$ electric-quadrupole matrix elements for the first 2^+ levels. In this Rapid Communication, direct measurements of a spherical shape in radioactive semimagic nuclei are reported for the first time.

A method for measuring the Coulomb excitation of RIBs using inverse kinematics ($A_{\text{projectile}} > A_{\text{target}}$) has been developed at the Holifield Radioactive Ion Beam Facility (HRIBF) [3]. With this method, scattered target nuclei are measured at forward angles relative to the beam direction (corresponding to backward angles in the center-of-mass frame) to provide a clean trigger for selecting the γ-ray transitions from the Coulomb-excited beam and to normalize the integrated beam current through Rutherford scattering. Preliminary $B(E2; 0_1{}^+ \to 2_1{}^+) = \langle 0_1||M(E2)||2_1\rangle^2$ results from HRIBF have been reported previously using this technique for neutron-rich ^{126,128,130,132,134}Sn RIBs [4].

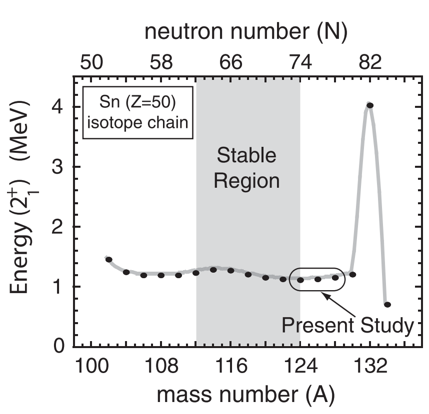

FIG. 1. The $2_1{}^+$ energies [2] of the Sn isotopic chain.

In the present study, ^{124}Sn(stable) and ^{126,128}Sn(unstable) are remeasured to obtain high-precision $\langle 0_1||M(E2)||2_1\rangle$ and $\langle 2_1||M(E2)||2_1\rangle$ matrix elements. This is the first report of measured $2_1{}^+$ static quadrupole moments, $Q(2_1{}^+) = 0.7579 \times \langle 2_1{}^+||M(E2)||2_1{}^+\rangle$, for the unstable Sn isotopes.

Beams of ^{124,126,128}Sn at an energy of 3 MeV per nucleon were studied by Coulomb excitation on two $\sim$1.2 mg/cm^2 targets: a natural ^{12}C target and a 90.5% enriched ^{50}Ti target. The energy loss of the ^{124}Sn beam (at 3 MeV per nucleon) through each target was measured by a Bragg detector at zero degrees and resulted in 82(1) MeV energy loss for the ^{12}C target and 58(2) MeV energy loss for the enriched ^{50}Ti target. Comparisons of experimental and simulated γ-ray Doppler shifts further support these measured energy losses. The ^{126,128}Sn RIBs were clean from isobaric contamination due to a chemical technique developed at HRIBF, which is based on the formation of the SnS$^+$ molecular ion [5]. The RIB intensities were $\sim 2 \times 10^6$ ^{126}Sn/s and 5×10^5 ^{128}Sn/s. However, only 81.1(21)% of the ^{128}Sn beam was in the ground state, $0_1{}^+$, with the remainder in the metastable 7^- state. This

*Present address: Nuclear Physics, US Department of Energy, SC-26/Germantown Building, 1000 Independence Ave., SW Washington, DC 20585.
†Present address: Instituto de Ciencias Nucleares, UNAM, AP 70-543, 04510 México, D.F., México.

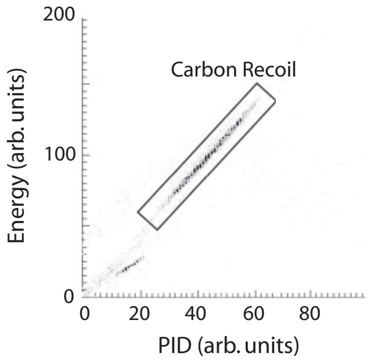

FIG. 2. A particle identification spectrum (PID) showing the recoiling carbon target nuclei in the HyBall array [6].

was determined by measuring the decay of the beam, stopped at the target position, on two separate occasions during the experiment, with consistent results.

Recoiling target nuclei were detected in the HyBall array [6] (cf. Fig. 2) using ring 2 (14°–28° relative to the beam direction and ten CsI crystals), ring 3 (28°–44° and 12 CsI crystals), and ring 4 (44°–60° and 12 CsI crystals). Coincident gamma rays were detected by 11 HPGe segmented clover detectors of the CLARION array [7] at angles of 90°(five clovers), 132°(four clovers), and 154°(two clovers) at a distance of 21.75 cm from the target foil with a total efficiency of 2.94(5)% at 1 MeV. The left-middle-right side channels of these segmented clover detectors were used to effectively give eight segments per clover (2 × 4 leaves). The experimental trigger required either a scaled-down particle singles or a particle-γ coincidence. The particle-gated γ-ray transitions of ^{124,126,128}Sn ($2_1{}^+ \rightarrow 0_1{}^+$) from Coulomb excitation are shown in Fig. 3. The relatively high efficiency of the particle-γ coincidence trigger and high resolution of CLARION provide an excellent tag of the $2_1{}^+$ states in ^{124,126,128}Sn.

The $E2$ matrix elements for ^{124,126,128}Sn can be approximated from the data using the following relation in second-order perturbation theory [8],

$$\frac{\sigma_{\mathrm{Coulex}}(2_1{}^+)}{\sigma_{\mathrm{Ruth}}} \approx A\langle 0_1||M(E2)||2_1\rangle^2[1+B\langle 2_1||M(E2)||2_1\rangle], \tag{1}$$

where $\sigma_{\mathrm{Coulex}}(2_1{}^+)$ is the $2_1{}^+$ Coulomb-excitation cross section, σ_{Ruth} is the Rutherford cross section, and A and B are scale factors dependent on the kinematics of the projectile and target combination. The scale factor B is relatively small for the low-Z ^{12}C target data ($B \sim 0.11$) but not for the relatively high-Z ^{50}Ti target data ($B \sim 0.46$). In the present study, the cross sections are calculated with the Coulex code GOSIA [9]. The GOSIA calculations are not limited to second-order perturbation theory [cf. Eq. (1)], which is particularly important for the determination of diagonal $E2$ matrix elements. Furthermore, the GOSIA calculations include the following corrections to the Coulex cross sections and γ-ray angular distributions [9]: dipole polarization correction, kinematic correction to the solid angle, nuclear deorientation (attenuation) correction, and finite-size gamma detector (attenuation) correction.

The $\langle 0_1||M(E2)||2_1\rangle$ matrix elements for ^{124,126,128}Sn are determined to be (+)0.403(7) eb, (+)0.356(11) eb, and

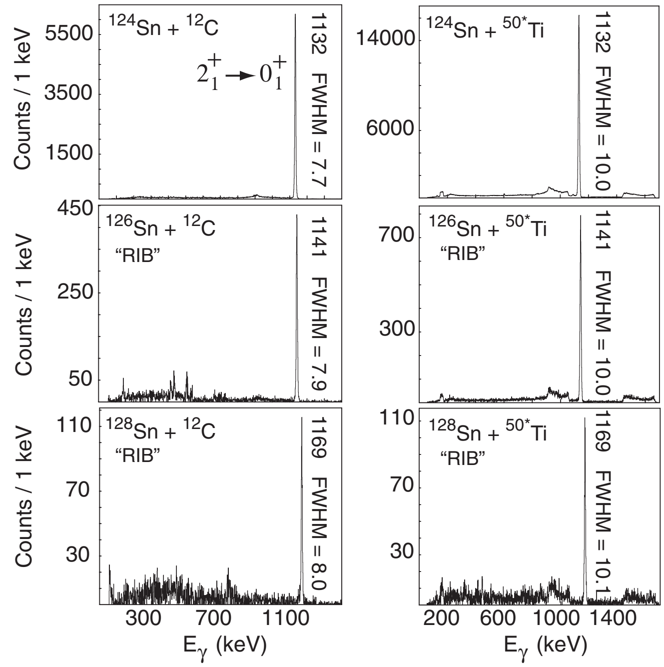

FIG. 3. The particle gated $2_1{}^+ \rightarrow 0_1{}^+$ γ-ray transitions of ^{124,126,128}Sn from the ^{12}C and enriched ^{50}Ti target data.

(+)0.282(9) eb, respectively. The ^{124}Sn value is in excellent agreement with the adopted value of (+)0.407(7) eb [2] and with the recent value of (+)0.385(19) eb from a direct lifetime measurement by Jungclaus *et al.* [10]. The ^{126,128}Sn values are consistent with preliminary results given in an earlier experiment by Radford *et al.* [4]. The errors in the present study are dominated by statistics (0.24%–2.5% error in transition matrix element) and the uncertainty in the absolute γ-ray efficiency (∼1.4% error in transition matrix element), but also include uncertainties in the target thickness, detector geometry, and beam purity. The $\langle 0_1||E2||2_1\rangle$ matrix elements decrease monotonically as the $N = 82$ shell closure is approached from $N = 74$ to 78, despite the near constancy in $E(2_1{}^+)$.

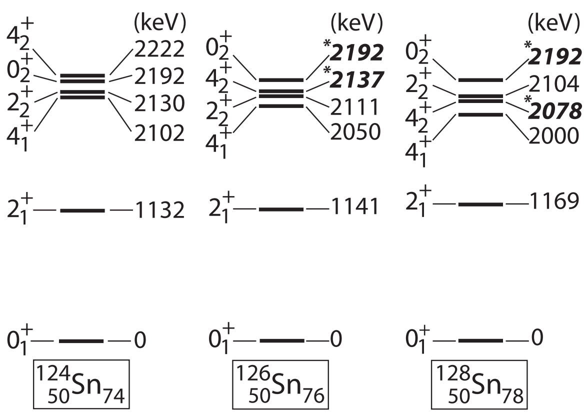

FIG. 4. Levels included in the Coulex analysis of $\langle 2_1{}^+||M(E2)||2_1{}^+\rangle$ "with higher-lying states" [2]. The four level energies with stars (*) are estimated from extrapolated systematics [2].

TABLE I. "Input" $E2$ matrix elements (in eb with no $i^\lambda = i^2 = -1$ phase) used in the Coulex analysis of $2_1{}^+$ for ^{124,126,128}Sn. A (±) sign is given for $\langle 0_1{}^+||M(E2)||2_2{}^+\rangle$ to indicate alteration of the sign of the quadrupole interference term, P_3, in Eq. (2); see text for details.

$Z = 50$	N	$\langle 0_1{}^+\|\|M(E2)\|\|2_2{}^+\rangle$	$\langle 2_1{}^+\|\|M(E2)\|\|0_2{}^+\rangle$	$\langle 2_1{}^+\|\|M(E2)\|\|2_2{}^+\rangle$	$\langle 2_1{}^+\|\|M(E2)\|\|4_1{}^+\rangle$	$\langle 2_1{}^+\|\|M(E2)\|\|4_2{}^+\rangle$
^{124}Sn	74	(±)0.0148(49)[a]	(+)0.183(31)	(+)0.5653(65)[a]	(+)0.398(25)[a]	(+)0.60(30)[a]
^{126}Sn	76	(±)0.0133(46)	(+)0.166(39)	(+)0.69(15)	(+)0.351(47)	(+)0.53(27)
^{128}Sn	78	(±)0.0117(46)	(+)0.150(46)	(+)0.76(27)	(+)0.273(88)	(+)0.50(27)

[a]Adopted experimental values [2]; extrapolation otherwise.

The $\langle 2_1||M(E2)||2_1\rangle$ matrix elements for ^{124,126,128}Sn can be extracted from the ^{50}Ti target data when combined with the results from the ^{12}C target data. However, the Coulex analysis of the heavier ^{50}Ti target data requires the inclusion of higher-lying states because of interference and virtual excitation effects on the $2_1{}^+$ Coulex cross sections. There are no observed γ-ray transitions from higher-lying states in the present study, but the effect of those states should be included in the Coulex analysis even if γ rays from those states are unobserved [11].

Figure 4 and Table I show the levels and input $E2$ matrix elements used in the Coulex analysis when including the effect of higher-lying states. While the majority of the energies are experimentally known [2], many of the $E2$ matrix elements are not known (at least for ^{126,128}Sn). The unknown transition $E2$ matrix elements are estimated from extrapolations of the adopted literature [2] (as a function of neutron number). The error bars assigned to these extrapolated values represent the uncertainty in the extrapolation. The unknown diagonal $E2$ matrix elements are excluded since there are no systematics from which to extrapolate, and their impact on the extracted $E2$ matrix elements is negligible (i.e., <0.001 eb impact). While these higher-lying states and their $E2$ matrix elements have no appreciable impact on the extracted $\langle 0_1||M(E2)||2_1\rangle$ values from the ^{12}C target data, they do impact the extracted $\langle 2_1||M(E2)||2_1\rangle$ values from the ^{50}Ti target data. Furthermore, because the $2_1{}^+$ state (where reorientation depends on $\langle 2_1||M(E2)||2_1\rangle$) experiences interference from the 0_1-2_2-2_1 path, both signs of the quadrupole interference term [9,12,13],

$$P_3 = \langle 0_1||M(E2)||2_1\rangle\langle 2_1||M(E2)||2_2\rangle\langle 2_2||M(E2)||0_1\rangle, \quad (2)$$

must be considered; the signs of the other matrix elements have no impact. No $i^\lambda = i^2 = -1$ phase (i.e., $i^\lambda\langle I'||M(E2)||I\rangle = -\langle I'||M(E2)||I\rangle$, which is sometimes included in the definition of $E2$ matrix elements [8]) is used in the present study. While the sign of P_3 can be experimentally determined, no measurement has been reported for ^{124,126,128}Sn.

The extracted $\langle 2_1||M(E2)||2_1\rangle$ matrix elements for ^{124,126,128}Sn are presented in Table II, both with and without higher-lying states included in the Coulex analysis. The uncertainties assigned to the input $E2$ matrix elements in Table I have been propagated into these results. The general effect of including the higher-lying states is that the $\langle 2_1||M(E2)||2_1\rangle$ matrix elements are systematically shifted by an average of 0.11 eb toward prolate deformation. However, both sets of results are consistent with zero deformation. The only other Sn Coulex study to include higher-lying states in the analysis

TABLE II. Summary of $E2$ matrix-element results (in eb with no i^λ phase) and the related $B(E2)$ e^{2}b^2 and $Q(2_1{}^+)$ eb values.

$Z = 50$	N	$\langle 0_1{}^+\|\|M(E2)\|\|2_1{}^+\rangle$	$\langle 2_1{}^+\|\|M(E2)\|\|2_1{}^+\rangle$ without high-lying	P_3	$\langle 2_1{}^+\|\|M(E2)\|\|2_1{}^+\rangle$[a] with high-lying
^{124}Sn	74	(+)0.403(7)	+0.04(9)	+	−0.08(11)
				−	−0.05(11)
^{126}Sn	76	(+)0.356(11)	+0.10(15)	+	−0.03(15)
				−	+0.01(15)
^{128}Sn	78	(+)0.282(9)	−0.02(24)	+	−0.17(25)
				−	−0.11(25)
$Z = 50$	N	$B(E2; 0_1{}^+ \to 2_1{}^+)$[b]	$Q(2_1{}^+)$[c] without high-lying	P_3	$Q(2_1{}^+)$[a,c] with high-lying
^{124}Sn	74	0.162(6)	+0.03(7)	+	−0.06(8)
				−	−0.04(8)
^{126}Sn	76	0.127(8)	+0.08(11)	+	−0.02(11)
				−	+0.01(11)
^{128}Sn	78	0.080(5)	−0.02(18)	+	−0.13(19)
				−	−0.08(19)

[a]Taking the higher-lying levels into account—cf. Fig. 4.
[b]$B(E2; 0_1{}^+ \to 2_1{}^+) = 5 \times B(E2; 2_1{}^+ \to 0_1{}^+) = \langle 0_1{}^+||M(E2)||2_1{}^+\rangle^2$.
[c]$Q(2_1{}^+) = 0.7579 \times \langle 2_1^+||M(E2)||2_1{}^+\rangle$.

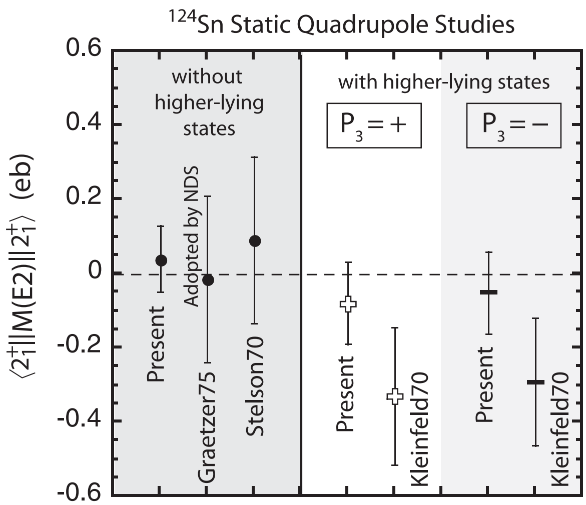

FIG. 5. ^{124}Sn studies of $\langle 2_1^+||M(E2)||2_1^+\rangle$ (eb), no $i^\lambda = i^2 = -1$ phase, with and without higher-lying states included in the Coulex analysis (Kleinfeld70 [14], Stelson70 [15], Graetzer75 [16]).

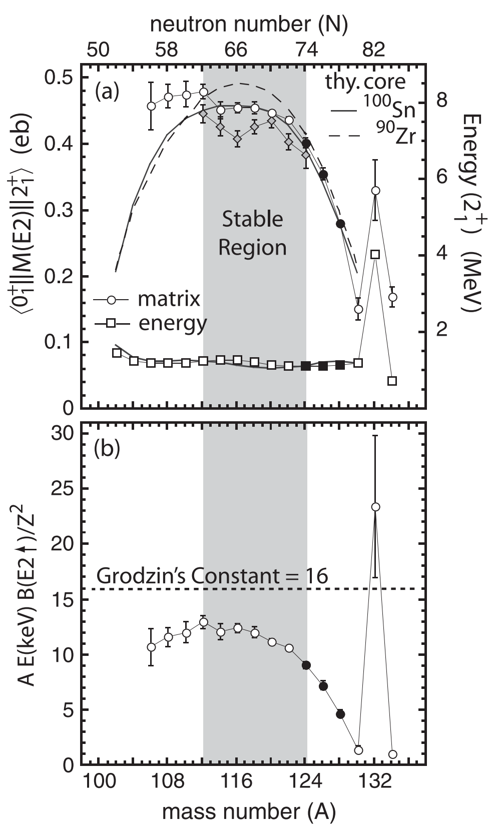

FIG. 6. The $2_1{}^+$ energy and $E2$ systematics for the Sn ($Z = 50$) isotopic chain. (a) $E(2_1{}^+)$ and $\langle 0_1||M(E2)||2_1\rangle$ systematics, where the ^{100}Sn/^{90}Zr core theory curves (solid and dashed, respectively) are from recent shell-model calculations by Banu *et al.* [17]. (b) The Grodzins product [20], which is empirically known to be $\sim$16 for open-shell nuclei. Black-filled points ($A = 124$, 126, 128) correspond to the present study; the white-filled (open) points are from the adopted [2] and recent literature [4,10,17,21–26] (i.e., weighted averages of experiments to date); the gray-filled diamonds are from a recent systematic study by Jungclaus *et al.* [10]. See text for details.

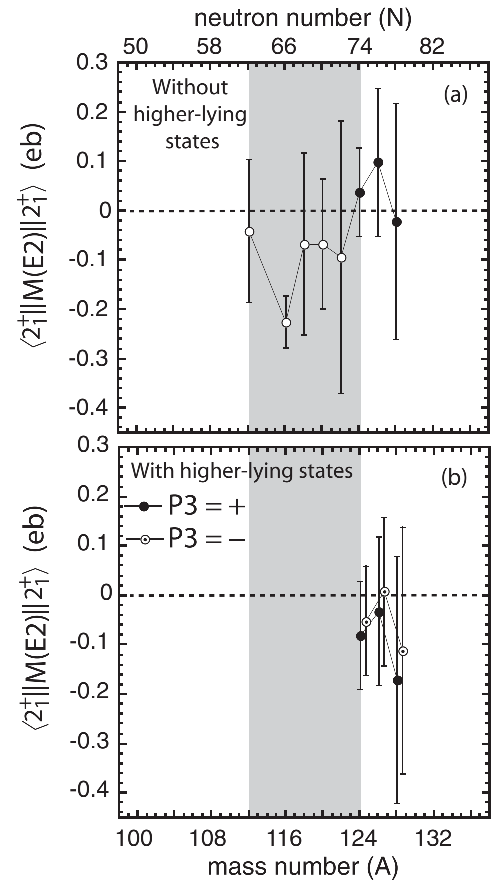

FIG. 7. The electric quadrupole moment systematics for the Sn ($Z = 50$) isotopic chain. (a) and (b) $\langle 2_1||M(E2)||2_1\rangle$ systematics without and with higher-lying states included in the Coulex analysis, respectively. Black-filled or black-dotted points ($A = 124$, 126, 128) correspond to the present study; the remaining points are from the adopted literature [2]. See text for details.

was by Kleinfeld *et al.* [14] for ^{116,124}Sn; this has not been included in the adopted literature [2]. Figure 5 shows all $\langle 2_1||M(E2)||2_1\rangle$ measurements to date for ^{124}Sn [14–16]. While Stelson *et al.* [15] and Graetzer *et al.* [16] did not include the effect of higher-lying states in their final results, they did comment that such an inclusion could alter their results by 0.1 eb, which agrees well with the $\sim$0.11 eb shift seen in the present study.

A summary of the present $E2$ matrix element results is given in Table II and displayed with the Sn systematics in Figs. 6 and 7. The $\langle 0_1||M(E2)||2_1\rangle$ matrix elements in Fig. 6(a) (white- and black-filled circles) show a global maximum at $A = 112$, $N = 62$, four neutrons away from the $N = 66$ midshell. As more neutrons are added toward the $N = 82$ shell closure, the $\langle 0_1||M(E2)||2_1\rangle$ matrix elements decrease (dramatically for $N = 74$ to 80), despite the near constancy in $E(2_1{}^+)$ [cf. Figs. 6(a) and 6(b)], and then show a sudden local maximum at $N = 82$, similar to the behavior observed near the doubly magic nucleus ^{208}Pb [2]. As neutrons are removed toward the $N = 50$ shell closure, the $\langle 0_1||M(E2)||2_1\rangle$ matrix elements show only a modest decline from the maximum at $N = 62$. $E2$ matrix elements for ^{102,104}Sn (i.e., the "mirror" of ^{130,128}Sn in that they are two and four neutrons away from a double-shell closure) would be very valuable for a better understanding of nuclear structure near ^{100}Sn. Indeed, because $N = Z$ for ^{100}Sn, anomalies in the neighboring $\langle 0_1||M(E2)||2_1\rangle$ systematics could arise from p-n interactions between protons and neutrons in similar orbits.

Recent shell-model calculations by Banu *et al.* [17] [cf. Fig. 6(a)], which are consistent with a generalized-seniority scheme [18], predict relatively constant $2_1{}^+$ energies and a parabolic trend in the $\langle 0_1||M(E2)||2_1\rangle$ matrix elements for $A = 102$–130. The agreement between theory (particularly with a ^{100}Sn core) and data for $A = 114$–128 is remarkable. The high level of agreement is most likely due, in part, to the filling (primarily) of a single-j orbital, i.e., $\nu h_{11/2}$. However, a recent direct-lifetime study of the stable Sn isotopes by Jungclaus *et al.* [10] has reported a nonparabolic trend in the $\langle 0_1||M(E2)||2_1\rangle$ matrix elements near the midshell region [cf. gray-filled diamonds in Fig. 6(a)], with a local minimum at the $N = 66$ midshell. It has been shown that this deviation from a parabolic trend at midshell is still consistent with a generalized-seniority scheme [19] and with the interpretation that a single-j orbital $\nu h_{11/2}$ is being primarily filled as the ^{132}Sn double-shell closure is approached.

Figure 6(b) shows the Grodzins product [20], which states that $E(2_1{}^+)$ and $B(E2; 0_1{}^+ \rightarrow 2_1{}^+) = \langle 0_1{}^+||M(E2)||2_1{}^+\rangle^2$ should be inversely proportional to each other (contrary to the generalized-seniority scheme). This product, which is an indicator of valence configuration space, is well known to be $\sim$16 and constant for $A > 12$ nuclei except for those at or adjacent to doubly closed shells. Indeed, the Grodzins product for the Sn chain is shown to be near 16 at midshell but not at or adjacent to the ^{132}Sn double-shell closure. Evidently, the valence configuration space decreases in size as ^{132}Sn is approached but it increases dramatically at ^{132}Sn.

The $\langle 2_1||M(E2)||2_1\rangle$ matrix elements without and with higher-lying states included in the Coulex analysis are shown in Figs. 7(a) and 7(b), respectively; this marks the first report on measured $2_1{}^+$ static quadrupole moments for unstable closed-shell nuclei. Despite the present measurements being performed with RIBs, the uncertainties are comparable with those from earlier stable beam experiments. The present results confirm that the unstable neutron-rich ^{126,128}Sn isotopes have a deformation consistent with zero.

The authors gratefully acknowledge fruitful discussions with D. Cline, A. B. Hayes, and J. L. Wood, and thank the HRIBF operations staff for developing and providing the radioactive beams used in this study. This research was sponsored by the Office of Nuclear Physics, US Department of Energy. This work was also supported in part by the US DOE under Contracts No. DE-AC05-76OR00033 (UNIRIB) and No. DE-FG02-96ER40963 (UTK).

[1] K. L. Jones *et al.*, Nature (London) **465**, 454 (2010).
[2] Evaluated Nuclear Structure Data File (ENSDF), [http://www.nndc.bnl.gov/ensdf/].
[3] D. C. Radford *et al.*, Phys. Rev. Lett. **88**, 222501 (2002).
[4] D. C. Radford *et al.*, Nucl. Phys. A **752**, 264c (2005).
[5] D. W. Stracener, Nucl. Instrum. Methods Phys. Res., Sect. B **204**, 42 (2003).
[6] A. Galindo-Uribarri, [http://www.phy.ornl.gov/hribf/research/equipment/hyball/].
[7] C. J. Gross *et al.*, Nucl. Instrum. Methods Phys. Res., Sect. A **450**, 12 (2000).
[8] K. Alder and A. Winther, *Coulomb Excitation* (Academic, New York, 1966), pp. 113–116 and 305.
[9] T. Czosnyka *et al.*, Bull. Am. Phys. Soc. **28**, 745 (1983); [http://www.pas.rochester.edu/~cline/Gosia/].
[10] A. Jungclaus *et al.*, Phys. Lett. B **695**, 110 (2011).
[11] T. Czosnyka *et al.*, Nucl. Phys. A **458**, 123 (1986).
[12] K. Kumar, Phys. Lett. B **29**, 25 (1969).
[13] J. M. Allmond, J. L. Wood, and W. D. Kulp, Phys. Rev. C **80**, 021303(R) (2009).
[14] A. M. Kleinfeld *et al.*, Nucl. Phys. A **154**, 499 (1970).
[15] P. H. Stelson *et al.*, Phys. Rev. C **2**, 2015 (1970).
[16] R. Graetzer *et al.*, Phys. Rev. C **12**, 1462 (1975).
[17] A. Banu *et al.*, Phys. Rev. C **72**, 061305(R) (2005).
[18] I. Talmi, Nucl. Phys. A **172**, 1 (1971).
[19] I. O. Morales, P. Van Isacker, and I. Talmi, Phys. Lett. B **703**, 606 (2011).
[20] L. Grodzins, Phys. Lett. **2**, 88 (1962).
[21] C. Vaman *et al.*, Phys. Rev. Lett. **99**, 162501 (2007).
[22] J. Cederkäll *et al.*, Phys. Rev. Lett. **98**, 172501 (2007).
[23] J. N. Orce *et al.*, Phys. Rev. C **76**, 021302(R) (2007); **77**, 029902(E) (2008).
[24] A. Ekström *et al.*, Phys. Rev. Lett. **101**, 012502 (2008).
[25] P. Doornenbal *et al.*, Phys. Rev. C **78**, 031303(R) (2008).
[26] R. Kumar *et al.*, Phys. Rev. C **81**, 024306 (2010).